COMMUNICATION

Check for updates

Zeolites with isolated-framework and oligomeric-extraframework hafnium species characterized with pair distribution function analysis†

Takayuki Iida,[ab] Koji Ohara,[c] Yuriy Román-Leshkov*[b] and Toru Wakihara [ID] *[a]

Zeolites containing framework heteroatoms (*e.g.*, Ti, Sn, and Hf) with open coordination sites behave as solid-state Lewis acids and exhibit remarkable catalytic properties unachievable with bulk oxides. However, direct evidence confirming the incorporation of such heteroatom species into the zeolite framework is difficult to obtain because of the limited number of analytical methods capable of discerning framework incorporation from extraframework species. In this work, the structural environments of hafnium (Hf) framework and extraframework species added post-synthetically into *BEA zeolites were analyzed using coupled pair distribution function (PDF) and diffuse reflectance (DR) UV-vis measurements. PDF analysis enabled the visualization and identification of framework and extraframework HfO_x species, both of which were undetectable by traditional X-ray and neutron diffraction methods. Reactivity data from the aldol condensation of benzaldehyde and acetone confirmed that framework Hf species are responsible for catalytic activity.

The substitution of tetrahedral group-IV metal cations (such as Ti^{4+}, Sn^{4+}, Zr^{4+}, and Hf^{4+}) into the crystallographic framework vertex sites (or T-sites) of zeolites, a group of inorganic microporous crystals composed of tetrahedral metal oxide units, leads to functional heterogeneous Lewis acid catalysts.[1] Among these catalysts, Hf-containing zeolites exhibit unique reactivity, as demonstrated for aldol condensation[2] and Meerwein–Ponndorf–Verley reduction[3] reactions, where Hf-containing zeolites outperform their Zr-, Ti-, and even Sn-containing zeolite counterparts both in terms of reactivity and selectivity for some substrates. However, conclusive structural evidence confirming that Hf cations are incorporated into and retained in the framework,

a Department of Chemical System Engineering, The University of Tokyo, 7-3-1 Hongo, Bunkyo-ku, Tokyo 113-8656, Japan. E-mail: wakihara@chemsys.t.u-tokyo.ac.jp

b Department of Chemical Engineering, Massachusetts Institute of Technology, 25 Ames Street, Cambridge, Massachusetts 02139, USA. E-mail: yroman@mit.edu

c Japan Synchrotron Radiation Research Institute/SPring-8, Kouto 1-1-1, Sayo-gun, Hyogo 679-5198, Japan

† Electronic supplementary information (ESI) available. See DOI: 10.1039/c8cp00464a

and demonstrating that these isolated species are the active Lewis acid sites has not been reported.

The aforementioned challenge is pervasive for most heteroatom-containing zeolites, especially in cases where the metal cations are inactive toward atoms-specific spectroscopic tools such as nuclear magnetic resonance (NMR) and electron spin resonance (ESR).[4–6] Titration techniques with various probe molecules[7,8] provide valuable information about the different types active sites, but several challenges including the possible interaction with the unintended adsorption sites (*e.g.*, structure defect sites), supra-stoichiometric adsorption, or the need to obtain unique molar extinction coefficients, in many cases, increase the complexity to interpret the results.[9] Extended X-ray absorption fine structure (EXAFS) analysis has emerged as an alternative tool to investigate the local structure of heteroatoms inside a solid.[10] However, the limited resolution in the radial distribution function calculated from EXAFS oscillation can be problematic for differentiating between the framework and the extraframework heteroatom species, as exemplified in a previous report on Zr-containing zeolites.[11] Reactivity measurements are also often used to verify the incorporation of heteroatoms; however, the possibility of the reaction being catalyzed by the extraframework species inside the zeolite micropores is sometimes overlooked. For example, in the isomerization of glucose, extraframework SnO_x clusters inside the hydrophobic zeolite micropores can also act as a solid base to drive the reaction *via* a different reaction mechanism[12] than the mechanism associated with the framework Lewis acid sites in Sn-containing *BEA zeolites.[13] Diffuse reflectance (DR) UV-vis measurements are also widely used to gain qualitative understanding of the presence of extraframework heteroatom species;[12] however, the difficulty in correlating with the absorption by nanosized oligomeric extraframework species makes full assignment of the observed absorption spectra on the basis of the framework heteroatom species difficult. Lastly, extra care must be taken when using the lattice parameter calculated by diffraction techniques to suggest the incorporation of heteroatoms because the extraframework species can expand the pore diameter and thus disturb the crystallographic information available by diffraction techniques.[14]

The pair distribution function (PDF), $G(r)$, is an alternative methodology for describing the structure of an analyte by presenting the probability of finding a certain interatomic distance within a unit volume.[15] An important difference between the PDF method and diffraction techniques is the ability to obtain structural information from the scattering of X-rays (or neutrons) instead of being limited to the information obtained from diffraction. Because of such features, nanostructures with a periodicity no larger than the unit-cell parameter can be measured, whereas diffraction can detect only structures with larger dimensions of ordering (multitude of unit cells in size).[16] Therefore, not only can PDFs depict structures from a distinctly different perspective than crystallography, but also can be applied to both crystalline and disordered materials, such as the amorphous intermediates present before zeolite crystallization.[17,18] An applied analysis method called the differential pair distribution function (d-PDF)[19] has been used to investigate the structure of some small nanoclusters/nanoparticles present on catalyst supports. The features of this analytical tool are expected to be useful for examining the extraframework heteroatom species that do not generate diffraction patterns as well as for discerning the structure of the heteroatom species inside the zeolite framework.

One challenge considered beforehand was that the signal from the isolated-framework sites would be too weak to provide sufficient scattering data for analysis. Therefore, in this work, Hf-containing *BEA zeolite was used as the model material because of the large X-ray scattering factor of Hf (the X-ray scattering factor of an element is proportional to its atomic number). Hf, with atomic number 72, has atomic properties similar to those of Zr because of the lanthanide contraction of atomic size (crystal atomic radii: Zr^{4+}, 73 pm; Hf^{4+}, 72 pm).[20] The *BEA zeolite, a crystal intermixture of BEA and BEB polymorphs (further details in Fig. S1, ESI†), is commonly used for catalytic reactions involving bulky substrates because of its large, three-dimensional pores and was chosen in the present work as the base topology for post-synthesis modifications.

In the present study, Hf-containing *BEA zeolites were prepared post-synthetically using a modified version of a previously reported method.[21] The post-synthesis route can produce zeolite catalysts with greater flexibility in the Hf composition as well as in the degree of incorporation,[21] when compared to the direct synthesis route.[2] Hf was first inserted into the dealuminated *BEA zeolites (DeAl-beta) using bis(cyclopentadienyl)hafnium(IV) dichloride ($Hf(Cp)_2Cl_2$) as a precursor, and the solid was subsequently calcined to remove the organic groups (product denoted as Hf-beta(post)). Dealumination was performed by acid treatment of the commercial aluminosilicate *BEA zeolite (Si/Al = 12.5) using concentrated (60 wt%) nitric acid. Although similar methods have been used to produce various heteroatom-containing zeolites,[21] the possibility of forming extraframework species is always present. Therefore, a second acid treatment was then performed on the as-prepared Hf-beta(post) using concentrated nitric acid (60 wt%) to remove possible extraframework HfO_2 species (samples denoted with suffix "_AT"). To prepare a sample that exclusively contained extraframework HfO_x species,
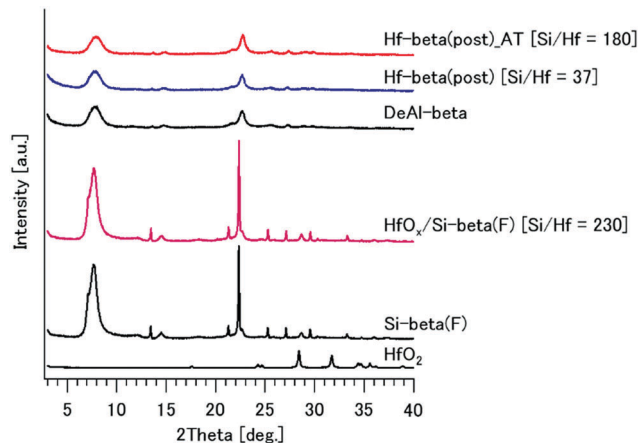

Fig. 1 XRD patterns of Hf-beta(post), Hf-beta(post)_AT, dealuminated *BEA zeolite (DeAl-beta), HfO_x/Si-beta(F), and Si-beta(F) in reference to HfO_2. The intensity values for HfO_2 were reduced to one-fourth of their original values. Diffraction peaks confirmed in the zeolite samples all originated from the *BEA zeolite crystal structure. The elemental compositions (Si/Hf) calculated from ICP-AES measurements are also shown in brackets [].

we used $Hf(Cp)_2Cl_2$ to impregnate a pure silica, defect-free *BEA zeolite prepared in fluoride media, denoted as HfO_x/Si-beta(F). Further synthetic and characterization details are summarized in the ESI.†

A comparison of the XRD patterns of Hf-beta(post), Hf-beta(post)_AT, and HfO_x/Si-beta(F) with the patterns of their parent zeolites confirmed the presence of *BEA crystals with crystallinities similar to those of the original crystals (Fig. 1). The HfO_2 phase was not detected via diffraction. The Si/Hf molar ratio is also shown in Fig. 1, and details of the elemental compositions of these catalysts are summarized in Table S1 (ESI†). N_2 physisorption measurements also verified that the crystallinity in terms of micropore volume was maintained throughout the treatment procedures (Table S2; isotherms in Fig. S2, ESI†).

Having confirmed the difficulty in differentiating these crystals by diffraction analyses, we carried out structural investigations based on PDF analyses. In addition to using monochromic synchrotron X-ray (61.4 keV), the obtained scattering data are normalized by the incident X-ray intensity during the calculation process to remove the influence of fluctuation in the beam intensity. Also, to assure high-quality data, for all samples, measurements were performed using long dwell times (for example, in the θ range where diffraction does not appear i.e. $\theta > 4°$, dwell time > 20 s with $\Delta\theta = 0.05°$). Thus, it was confirmed from the Faber–Ziman total structure factors, $S(Q)$, used for the calculation of PDFs (summarized in Fig. S3, ESI†) that the measurements are conducted under conditions where there is little influence on the error range by the dwell time. The PDFs of HfO_x/Si-beta(F) and Si-beta(F) are shown in Fig. 2(a). The peaks in the PDF of Si-beta(F), $G_{Si-beta(F)}(r)$, depict the probability of finding the given atomic distance in the siliceous *BEA crystal structure. For example, the correlation peaks at $r = 1.61$, 2.6, and 3.1 Å correspond to the nearest-neighbor Si–O, O–Si–O, and Si–O–Si interatomic distances.
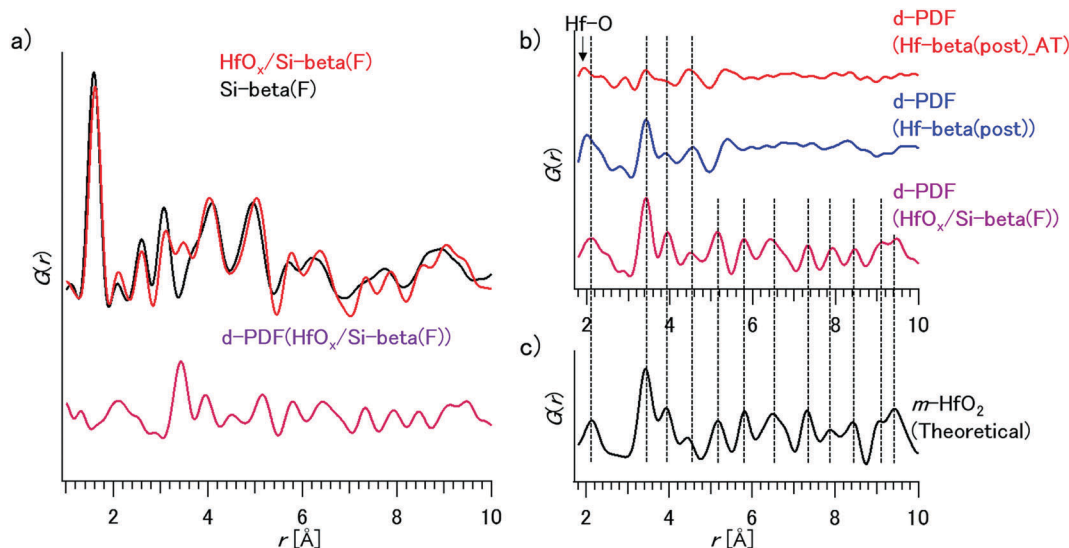
Fig. 2 (a) The d-PDF calculation of HfO$_x$/Si-beta(F) (pair distribution function), $G(r)$, of HfO$_x$/Si-beta(F) and Si-beta(F), and the difference between these two PDFs (d-PDF); (b) d-PDF results for Hf-beta(post)_AT, Hf-beta(post), and HfO$_x$/Si-beta(F); (c) theoretical PDF of monoclinic HfO$_2$, as calculated using the PDFgui software.[24]

We carried out a d-PDF analysis (shown in Fig. 2(a)) to highlight some of the subtle differences between the PDFs of HfO$_x$/Si-beta(F) and Si-beta(F). The d-PDF method is based on the linear feature of PDF, which enables differential calculations between the PDFs, $G(r)$, to extract the structure of a minority element in a binary phase admixture (a detailed explanation of the method is summarized in the ESI†). For example, in the context of this work, the PDF describing the structure of oligomeric HfO$_x$ species in HfO$_x$/Si-beta(F), $G_{Hf-}(r)$, can be calculated from eqn (1), which corresponds to the difference between the PDFs of HfO$_x$/Si-beta(F) and Si-beta(F):

$$x_B G_{Hf-}(r) = G_{HfO_x/Si\text{-}beta(F)}(r) - x_A G_{Si\text{-}beta(F)}(r) \qquad (1)$$

where x_A and x_B are coefficients. Theoretically, the same calculation should provide the structural environment around Hf in the zeolite framework T-sites when the calculation is performed for zeolites with Hf inside their framework. The calculated d-PDF results for all of the samples are provided in Fig. 2(b).

As anticipated, HfO$_x$ species were identified in the d-PDF of HfO$_x$/Si-beta(F). Notably, the PDF is capable of distinguishing various HfO$_2$ phases (*e.g.*, monoclinic, cubic, and orthorhombic) on the basis of the differences in the relative positions of Hf and O atoms reflected in distinct PDFs (Fig. S4, ESI†). The d-PDF of HfO$_x$/Si-beta(F) was referenced with the theoretical PDF of monoclinic HfO$_2$ (m-HfO$_2$) for "phase" identification (Fig. 2(c)) after the peak positions and the relative intensities were compared with the theoretical PDFs of other HfO$_2$ phases. Further, the deconvolution of the theoretical PDF of m-HfO$_2$ clarified that most correlations originate from Hf–Hf and Hf–O correlations because of the high X-ray scattering factor of Hf (Fig. S5, ESI†).

Likewise, when the d-PDF calculation was performed for Hf-beta(post) (Fig. 2(b)), the presence of correlations corresponding to m-HfO$_2$ was confirmed in the region $3 \leq r \leq 6$ Å. The lack of correlations corresponding to m-HfO$_2$ beyond 6 Å

shows that the size of the nanoclusters is smaller than this value. This result implies that the extraframework HfO$_x$ nanoclusters can be formed and stabilized inside the zeolite pores.[22] Such correlation peaks were also confirmed in the d-PDF of Hf-beta(post)_AT; however, the areas of the peaks were smaller than those of Hf-beta(post) signifying that the acid treatment was effective at removing extraframework clusters. Interestingly the d-PDF of Hf-beta(post)_AT showed correlations different from those of HfO$_x$/Si-beta(F). Specifically, the correlation at approximately $r = 2.0$ Å, which corresponds to the nearest-neighbor Hf–O correlation (shown with an arrow in Fig. 2(b)), was at a shorter distance than in the d-PDF of HfO$_x$/Si-beta(F). Although this correlation can be influenced by the termination ripple artifacts formed during the Fourier transformation used to obtain the PDFs,[23] the fact that the position of the nearest-neighbor oxygen appears at a shorter distance implies the presence of tetrahedral Hf species in comparison to the octahedral Hf in m-HfO$_2$. Overall, these findings indicate that the correlations observed in the d-PDF of Hf-beta(post) and Hf-beta(post)_AT can originate from the interatomic correlations between framework Hf and the surrounding Si and O atoms in the zeolite structure and/or from the components of the extraframework HfO$_x$ nanoclusters. The ratio between the framework and the extraframework Hf cannot be fully determined only from the d-PDF results of these zeolite samples because of the possible overlap of the correlation peaks.

To justify the correlation between framework Hf and the zeolite in the positions observed in the d-PDF of Hf-beta(post) and Hf-beta(post)_AT, the d-PDF was compared with that of a different heteroatom-containing *BEA zeolite. An identical post-synthetic treatment was used to prepare *BEA zeolites with Sn incorporated inside the framework (including the acid treatment, the product was designated as Sn-beta(post)_AT), and the d-PDF is shown in reference to that of Hf-beta(post)_AT (Fig. 3).

7916 | *Phys. Chem. Chem. Phys.*, 2018, **20**, 7914–7919
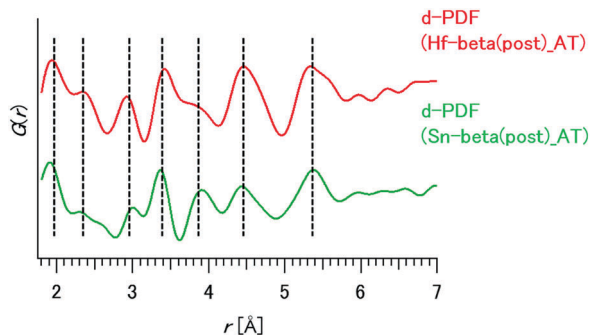
This journal is © the Owner Societies 2018

Fig. 3 Comparison of the d-PDF between Hf-beta(post)_AT and Sn-beta(post)_AT. The d-PDF of Hf-beta(post)_AT was offset, and the corresponding peaks in the region between $1.8 \leq r \leq 6$ Å are shown with dotted lines as visual guides.

A comparison with the theoretical PDF of SnO_2 (cassiterite, shown in Fig. S6, ESI†) showed that the correlations of Sn-beta(post)_AT were completely different from the correlations of SnO_2. Notably, the positions of the d-PDF correlations for Hf-beta(post)_AT and Sn-beta(post)_AT were observed at similar distances (the crystal atomic radii of tetrahedral Sn^{4+} and Hf^{4+} are similar, 69 and 72 pm, respectively),[20] providing further evidence that the d-PDF can represent the peripheral environment of the heteroatoms incorporated inside the zeolite framework. Again, because of the possible overlap in the correlations, the ratio of the framework and the extraframework Hf species cannot be fully determined even at this stage.

Further characterization based on DR UV-vis measurements, another bulk characterization tool that can investigate the different Hf species, was performed (Fig. 4). The presence of a broad absorption band between 250 and 500 nm was only confirmed in the spectra of Hf-beta(post) and HfO_x/Si-beta(F), whereas such absorption was not present in the spectrum of Hf-beta(post)_AT. Because HfO_x/Si-beta(F) is a sample that exclusively possesses extraframework HfO_x, and because such extraframework species can be expected to be present in Hf-beta(post), this peak was assigned to the absorption by the
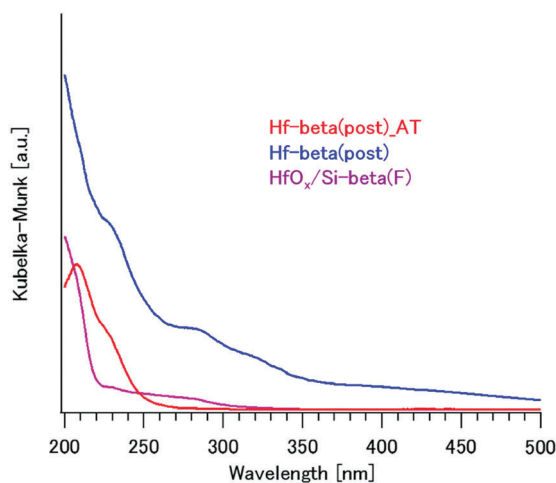
oligomeric extraframework HfO_x species. This assignment is in agreement with the d-PDF results. Indeed, bulk HfO_2 is known to show an absorption peak at 210 nm (Fig. S7, ESI†), and the reason for the shift to the 250–500 nm region remains a topic for future investigations. By contrast, only the absorption between 200 and 240 nm was confirmed in the spectrum of Hf-beta(post)_AT. Because Hf-beta(post)_AT was the product obtained after an acid treatment that removed the oligomeric HfO_x from Hf-beta(post), as confirmed from the DR UV-vis spectra, the absorption between 200 and 240 nm was assigned to the framework Hf species. These assignments substantiate the report by Lewis et al.[2] and Mahmound et al.,[25] which makes the assignments of the DR UV-vis based on the spectra of zeolite catalysts that were prepared differently having different activities for Lewis acid-catalyzed reactions.[2,25] The small shouldering peak at 225 nm was also confirmed and was tentatively assigned to the octahedral Hf that partially bonds with the zeolite framework because this peak was still present after the acid treatment that removed the HfO_x nanoclusters. Thus, in conjunction with the DR UV-vis results, the correlations observed in the d-PDF of Hf-beta(post)_AT can be conclusively assigned to Hf atoms incorporated into the zeolite framework.

Roman-Leshkov et al. demonstrated that the aldol condensation between benzaldehyde and acetone (Fig. 5), can be catalyzed by the Lewis acid sites of Hf inside the zeolite following a soft-enolization route that results in a high selectivity values toward the monocondensed product (product **a**) over the bicondensed product (product **b**).[2] We conducted this reaction at identical catalyst loadings and reaction times to determine whether the framework Hf or the extraframework HfO_x nanoclusters are the active sites (Table 1). Despite the fact that Hf-beta(post) possessed five times more Hf than Hf-beta(post)_AT, both catalysts were equally selective and active toward the formation of the monocondensed product (product **a**). Because the d-PDF results indicated that only nanoclusters with particle sizes smaller than 6 Å are present in Hf-beta(post), the formation of bulk extraframework HfO_x species with small surface areas and few active sites can be ruled out. These results confirm, as suggested in the original paper,[2] that the framework Hf atoms are indeed the active site for the Lewis catalyzed aldol condensation.

In summary, we applied PDF analysis to post-synthetically prepared Hf-containing *BEA zeolites to discriminate the framework and the extraframework species in Hf-containing zeolites. The results provided unequivocal evidence of Hf incorporation into the crystallographic framework T-sites, as well as the visualization of the extraframework HfO_x species. Further, coherency and complementarity with the DR UV-vis

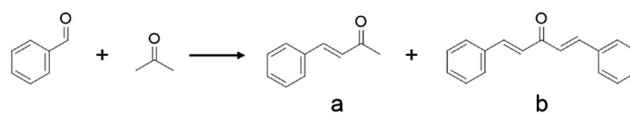Fig. 4 DR UV-vis spectra of various Hf zeolites.

Fig. 5 Reaction scheme for the aldol condensation between benzaldehyde and acetone to form benzylacetone (product **a**, monocondensed product) and diphenylpenta-3-none (product **b**, bicondensed product).

Table 1 Results for the aldol condensation between benzaldehyde and acetone (conversion and yield of product a (monocondensed product))

Catalyst	Hf/(Hf + Si) [mol%]	Conversion [%]	Yield [%]
Hf-beta(post)	2.6	20	14
Hf-beta(post)_AT	0.54	25	16

Reaction conditions: reaction solution: 1 g (benzaldehyde 1 mmol L^{-1}, 3 equiv. acetone, solvent: toluene); reaction temperature: 80 °C; reaction period: 30 min; catalyst: 40 mg. Trace formation of the bicondensed product was confirmed.

results were confirmed, enabling the assignment of absorption peaks based on visualized Hf structures. Finally, experimental results to assign the framework Hf species to be the main active site for aldol condensation was acquired by comparing the catalytic activity of a zeolite that contains both framework and extraframework Hf, and another in which the latter was removed. This work is the first to shed light on how extraframework heteroatom oxide species that are not detected by X-ray diffraction actually exist inside the admixture with the *BEA zeolite crystals. Complementing existing reports of the incorporation of different metals into the zeolite framework, the current work provides a unique, powerful tool for articulating the catalytically active structure inside zeolite catalysts.

Conflicts of interest

There are no conflicts to declare.

Acknowledgements

References

1 H. Y. Luo, J. D. Lewis and Y. Román-Leshkov, Lewis Acid Zeolites for Biomass Conversion: Perspectives and Challenges on Reactivity, Synthesis, and Stability, *Annu. Rev. Chem. Biomol. Eng.*, 2016, **7**, 663–692.
2 J. D. Lewis, S. Van De Vyver and Y. Román-Leshkov, Acid-Base Pairs in Lewis Acidic Zeolites Promote Direct Aldol Reactions by Soft Enolization, *Angew. Chem., Int. Ed.*, 2015, **54**, 9835–9838.
3 H. Y. Luo, D. F. Consoli, W. R. Gunther and Y. Román-Leshkov, Investigation of the reaction kinetics of isolated Lewis acid sites in Beta zeolites for the Meerwein-Ponndorf-Verley reduction of methyl levulinate to γ-valerolactone, *J. Catal.*, 2014, **320**, 198–207.
4 A. Tuel, J. Diab, P. Gelin, M. Dufaux, J.-F. Dutel and Y. Ben Taarit, EPR evidence for the isomorphous substitution of titanium in silicalite structure, *J. Mol. Catal.*, 1990, **63**, 95–102.
5 M. Moliner, Y. Román-Leshkov and M. E. Davis, Tin-containing zeolites are highly active catalysts for the isomerization of glucose in water, *Proc. Natl. Acad. Sci. U. S. A.*, 2010, **107**, 6164–6168.
6 P. Wolf, M. Valla, A. J. Rossini, A. Comas-Vives, F. Nfflçez-Zarur, B. Malaman, A. Lesage, L. Emsley, C. Copøret and I. Hermans, NMR Signatures of the Active Sites in Sn-β Zeolite, *Angew. Chem., Int. Ed.*, 2014, **53**, 1–6.
7 S. Roy, K. Bakhmutsky, E. Mahmoud, R. F. Lobo and R. J. Gorte, Probing lewis acid sites in Sn-Beta zeolite, *ACS Catal.*, 2013, **3**, 573–580.
8 V. L. Sushkevich, I. I. Ivanova and A. V. Yakimov, Revisiting Acidity of SnBEA Catalysts by Combined Application of FTIR Spectroscopy of Different Probe Molecules, *J. Phys. Chem. C*, 2017, **121**, 11437–11447.
9 R. Bermejo-Deval, R. S. Assary, E. Nikolla, M. Moliner, Y. Román-Leshkov, S.-J. Hwang, A. Palsdottir, D. Silverman, R. F. Lobo, L. A. Curtiss and M. E. Davis, Metalloenzyme-like catalyzed isomerizations of sugars by Lewis acid zeolites, *Proc. Natl. Acad. Sci. U. S. A.*, 2012, **109**, 9727–9732.
10 J. A. van Bokhoven and C. Lamberti, Structure of aluminum, iron, and other heteroatoms in zeolites by X-ray absorption spectroscopy, *Coord. Chem. Rev.*, 2014, **277–278**, 275–290.
11 J. Wang, K. Okumura, S. Jaenicke and G. K. Chuah, Post-synthesized zirconium-containing beta zeolite in Meerwein-Ponndorf-Verley reduction: pros and cons, *Appl. Catal., A*, 2015, **493**, 112–120.
12 R. Bermejo-Deval, R. Gounder and M. E. Davis, Framework and extraframework tin sites in zeolite beta react glucose differently, *ACS Catal.*, 2012, **2**, 2705–2713.
13 Y. Román-Leshkov, M. Moliner, J. A. Labinger and M. E. Davis, Mechanism of Glucose Isomerization Using a Solid Lewis Acid Catalyst in Water, *Angew. Chem., Int. Ed.*, 2010, **49**, 8954–8957.
14 L. B. McCusker, Zeolite Crystallography. Structure Determination in the Absence of Conventional Single-Crystal Data, *Acta Crystallogr., Sect. A: Found. Crystallogr.*, 1991, **47**, 297–313.
15 T. Proffen, S. J. L. Billinge, T. Egami and D. Louca, Structural analysis of complex materials using the atomic pair distribution function – a practical guide, *Z. Kristallogr.*, 2003, **218**, 132–143.
16 S. J. L. Billinge and I. Levin, The problem with determining atomic structure at the nanoscale, *Science*, 2007, **316**, 561–565.
17 T. Wakihara, S. Kohara, G. Sankar, S. Saito, M. Sanchez-Sanchez, A. R. Overweg, W. Fan, M. Ogura and T. Okubo, A new approach to the determination of atomic-architecture of amorphous zeolite precursors by high-energy X-ray diffraction technique, *Phys. Chem. Chem. Phys.*, 2006, **8**, 224–227.
18 T. Umeda, H. Yamada, K. Ohara, K. Yoshida, Y. Sasaki, M. Takano, S. Inagaki, Y. Kubota, T. Takewaki, T. Okubo

7918 | *Phys. Chem. Chem. Phys.*, 2018, **20**, 7914–7919

This journal is © the Owner Societies 2018

and T. Wakihara, Comparative Study on the Different Interaction Pathways between Amorphous Aluminosilicate Species and Organic Structure-Directing Agents Yielding Different Zeolite Phases, *J. Phys. Chem. C*, 2017, **121**, 24324–24334.

19 K. W. Chapman, P. J. Chupas and T. M. Nenoff, Radioactive iodine capture in silver-containing mordenites through nanoscale silver iodide formation, *J. Am. Chem. Soc.*, 2010, **132**, 8897–8899.

20 R. D. Shannon, Revised effective ionic radii and systematic studies of interatomic distances in halides and chalcogenides, *Acta Crystallogr., Sect. A: Cryst. Phys., Diffr., Theor. Gen. Crystallogr.*, 1976, **32**, 751–767.

21 J. C. Vega-Vila, J. W. Harris and R. Gounder, Controlled insertion of tin atoms into zeolite framework vacancies and consequences for glucose isomerization catalysis, *J. Catal.*, 2016, **344**, 108–120.

22 T. Iida, M. Shetty, K. Murugappan, Z. Wang, K. Ohara, T. Wakihara and Y. Román-Leshkov, Encapsulation of molybdenum carbide nanoclusters inside zeolite micropores enables synergistic bifunctional catalysis for anisole hydrodeoxygenation, *ACS Catal.*, 2017, **7**, 8147–8151.

23 M. M. Martínez-Iñesta and R. F. Lobo, Investigation of the structure of platinum clusters supported in zeolite beta using the pair distribution function, *J. Phys. Chem. C*, 2007, **111**, 8573–8579.

24 C. L. Farrow, P. Juhas, J. W. Liu, D. Bryndin, E. S. Božin, J. Bloch, T. Proffen and S. J. L. Billinge, PDFfit2 and PDFgui: computer programs for studying nanostructure in crystals, *J. Phys.: Condens. Matter*, 2007, **19**, 335219.

25 E. Mahmoud, J. Yu, R. J. Gorte and R. F. Lobo, Diels-Alder and Dehydration Reactions of Biomass-Derived Furan and Acrylic Acid for the Synthesis of Benzoic Acid, *ACS Catal.*, 2015, **5**, 6946–6955.